2003

Development and implementation of fine structure aerosol spectrum coagulation kernels and deposition mechanisms using advanced nodal method in the CAEROT code

HyeongKae Park
Louisiana State University and Agricultural and Mechanical College, hpark1@lsu.edu

DEVELOPMENT AND IMPLEMENTATION OF FINE STRUCTURE AEROSOL SPECTRUM COAGULATION KERNELS AND DEPOSITION MECHANISMS USING ADVANCED NODAL METHOD IN THE CAEROT CODE

A Thesis

Submitted to the Graduate Faculty of the
Louisiana State University and
Agricultural and Mechanical College
in partial fulfillment of the
requirements for the degree of
Master of Science

in

The Department of Physics and Astronomy

by
HyeongKae Park
B.S., University of Oregon, 2000
B.S., University of Oregon, 2001
August, 2003

TABLE OF CONTENTS

LIST OF TABLES

LIST OF FIGURES

ABSTRACT

Aerosol transport in confined spaces was studied via numerical simulation using the dynamic aerosol equation, which is Boltzmann's transport equation at the hydrodynamic limit. Until recent years, there existed no comprehensive computational tool to predict the spatial distribution and time evolution of aerosol size spectrum. A previously developed code, INDASOL3D, solves the dynamic aerosol equation by using a homogenized control-volume based finite difference method applying the group sectional method on the coagulation dynamics. However, quantitative correctness has not been satisfactory.

In this thesis, two new codes (SAEROSA, and CAEROT) were developed**.** SAEROSA computes the time evolution of the size spectrum in a spatially homogenized aerosol due to coagulation and deposition with user defined arbitrary group sectionalization. CAEROT computes space and time dependent aerosol size spectrum in an enclosed space by solving the lumped parameter integral transport equation along stream tubes. Compared to INDASOL3D, more comprehensive aerosol physics and improved numerical methods were included into CAEROT to resulting in a better prediction. SAEROSA was benchmarked against an existing code, MAEROS, while CAEROT was validated against experimental data obtained at the LSU Nuclear Science Center. Both codes give good results quantitatively and qualitatively**.**

CHAPTER 1. INTRODUCTION

1.1. MOTIVATION AND OBJECTIVES

The study and application of aerosol dispersion in enclosed spaces are of significant interest to the Health Physicist. For example, nuclear reactor accidents or fuel production laboratory accidents may release radioactive, or otherwise toxic airborne particles. Inhalation of these particles may cause adverse health effects. In addition, according to the US Environmental Protection Agency, people are more likely to be exposed to hazardous materials indoors than outdoors. The detailed knowledge of the spatial and temporal aerosol distribution in a confined space is necessary for the efficient placement of the air monitoring system, and for the risk analysis and the emergency planning in radiation worker protection.

An individual's inhalation exposure directly relates to the concentration of the aerosol in the breathing zone. The aerosol distribution is greatly affected by the room geometry and the airflow patterns. The consequence assessment of an incident is difficult to generalize, and it must be done for each specific geometry. However, experimental studies often require large efforts and costs. In addition, sometimes it is impossible to reproduce an exact geometry or situation, in which case they are often replaced by some simplified models. Thus, the computational modeling of aerosol transport is desirable.

The main objective of this research is to develop a comprehensive computational tool to predict the spatial and temporal evolution of aerosol concentration, deposition, and particle size distribution under given initial and boundary conditions in a confined space. A new code, CAEROT, was written to treat the dynamic aerosol transport. This, in turn was coupled with an

external computational fluid dynamics (CFD) code to obtain detailed velocity profiles as input to CAEROT. The new code was verified using existing experimental data. Part of CAEROT is another new code, SAEROSA, which treats coagulation and deposition, and can be run independently.

1.2. PREVIOUS WORK

Fundamental development of the motion of particles in fluid was done by Fuchs[1]. The theory of aerosol transport and related topics are discussed in Williams[2]. These two books describe the fundamental concepts and the formulation of aerosol transport.

The coagulation mechanism is a unique characteristic of aerosol transport. The Brownian coagulation was studied theoretically by Sitarski and Seinfeld [3], and an expression of the Brownian coagulation kernel as function of particle size was derived. Several mathematical coagulation models were compared by Seigneur et. al.[4]. Both continuous and sectional representations of aerosol size spectrum were compared in terms of computational cost and its accuracy. Detailed sectional treatment of aerosol property was presented by Gelbard and Seinfeld [5]. Discrete coagulation kernels using both geometric constraint and arbitrary sectionalization, and parameterization of the aerosol properties were derived therein.

Understanding of the deposition mechanism is crucial for the correct modeling of aerosol removal. Indoor turbulent deposition onto smooth surface was studied by Nazaroff [6]. Brownian deposition model of small particles in turbulent flow was studied by Davies[7]. Thermophoretic deposition correlation onto cold plate is done by Tsai, and Liang[8]. A comprehensive experimental study of indoor spatial variation of deposition was done by Sajo, Zhu, and Courtney[9], which showed that aerosol concentration distribution does not always follow airflow patterns.

Spatial aerosol dispersion experiments due to the influence of geometry and ventilation rate were done by Whicker, et al [10], that showed the importance of knowing the turbulent velocity distribution. Study of air monitor placement in a plutonium facility was done by Whicker et. al. [11]. However, no reliable 3-D computational model for confined areas has been available heretofore.

1.3. ORGANIZATION OF THIS THESIS

The mathematical development of aerosol transport is presented in Chapter 2. Discretization methods of independent variables, nodal methods, and the importance of the proper sectionalization are also discussed there as applied to the development of CAEROT. Chapter 3 discusses the benchmarking of a new coagulation/deposition code as applied to a well-mixed chamber. The developed code (SAEROSA) was benchmarked against an existing code (MAEROS) in two different time scales. Chapter 4 deals with the validation of CAEROT using an environmental chamber experiment. Sensitivity study against node size and velocity, and capabilities of the developed code are discussed in this chapter. Chapter 5 presents the conclusions of this research and suggests further work.

CHAPTER 2. MATHEMATICAL MODEL DEVELOPMENT OF AEROSOL DYNAMICS

2.1. AEROSOL CHARACTERISTICS AND DISTRIBUTION FUNCTION

An aerosol consists of particles suspended in gas. It is usually stable for at least a few seconds. The typical diameter range of interest is 10^{-8} m to 10^{-3} m. We are interested in the bulk behavior of aerosols in most applications. Thus, the aerosol is often characterized in terms of mass [μg/cc], volume [μm^3/cc], or number concentration [particle/cc]. The motion of the aerosol is complex: it is determined by both internal forces such as Brownian motion, and external forces such as gravitational force, fluid velocity field, and electrostatic force. The size of the aerosol particle is an important parameter that determines its motion. However, it may change if it collides with another particle. Various applications of aerosol transport require three important variables: size, time and spatial distribution. Since the size range of interest usually spans several orders of magnitude, the aerosol number distribution function, n(d,t) is often described by a log-normal distribution. A log-normal distribution function for particle diameter may be written as follows:

$$n(d,t) = \frac{N(t)}{\sqrt{2\pi}\,\ln(\sigma_g)d}\exp\left[-\frac{\{\ln(d)-\ln(d_m)\}^2}{2(\ln\sigma_g)^2}\right] \quad \textbf{(1)}$$

Where σ_g is geometric standard deviation;
d_m is median diameter of aerosol;
N(t) is the total number of particles as function of time.

Other aerosol properties, such as volume distribution, are also our interest. These may be expressed in terms of the number distribution, the volume of particles (v), and two parameters α and γ. Gelbard and Seinfeld [5] describe several aerosol properties in terms of these parameters. Let q(d,t) be a differential aerosol property defined as:

$$q(d, t) = \alpha\, v^{\gamma} n(d, t) \tag{2}$$

and the total aerosol property may be written as:

$$Q(t) = \int_0^{\infty} q(v, t)dv \tag{3}$$

For example, for α=1, γ=1, q(d,t) represents the aerosol volume distribution, and for α=1,γ=0, q(d,t) represents the aerosol number distribution. It is also possible to use a different independent variable than the particle diameter. For example, if the volume of the particle is the independent variable, then equation (1) becomes:

$$\begin{aligned} n(v, t) &= \frac{N(t)}{\sqrt{2\pi}\,\ln(\sigma_{g,v})v} \exp\left[- \frac{\{\ln(v) - \ln(v_m)\}^2}{2(\ln \sigma_{g,v})^2} \right] \\ \sigma_{g,v} &= \sigma_g^3 \\ v_m &= \frac{\pi\, d_m^3}{6} \end{aligned} \tag{1a}$$

Here, $\sigma_{g,v}$ is the geometric standard deviation of particle volume, and
v_m is the median volume of the number distribution.

It seems that there is a confusion in the way some of the literature describes the aerosol distribution functions. Since the distribution function is often observed via experiments and not derived by mathematical means, some investigators use a log-normal distribution to represent any aerosol property of interest. However, if number distribution is expressed by equation (1), and if parameter γ in equation (2) is not zero, then the aerosol property, q(d,t), will not possibly have a log-normal distribution. In addition, many publications confuse the mean with the median.

2.2. THE DYNAMIC EQUATION OF AEROSOL TRANSPORT

In order to predict the distribution of the aerosol property, the aerosol transport equation must be solved. The aerosol transport equation is Boltzmann's transport equation in the

hydrodynamic limit due to the appearance of convective motion. The dynamic equation of aerosol transport has the terms describing particle behavior in the environment due to extraneous forces acting on particles, particle-particle interactions, diffusion, condensation-evaporation, and thermophoresis.

$$\frac{\partial q(v,\vec{r},t)}{\partial t} + \nabla \cdot [\vec{U}(v,\vec{r},t)q(v,\vec{r},t)] - \nabla \cdot [D(v,\vec{r},t)\nabla q(v,\vec{r},t)] = \left.\frac{\partial q(v,\vec{r},t)}{\partial t}\right|_{growth} + \left.\frac{\partial q(v,\vec{r},t)}{\partial t}\right|_{coag} + S(v,\vec{r},t) \quad (4)$$

The above equation consists of five different interaction mechanisms. The first term of the left hand side (LHS) is total rate of change in the differential aerosol property having size v, at location, **r**, with respect to time, t. The second term of the LHS is a convective transport term due to the ambient velocity field U(v,r,t), assuming non-slip condition. The third term is a diffusion term as expressed by Fick's law. The first term in the right hand side (RHS) is the rate of change due to condensation and evaporation. The second term in the RHS is the rate of change in the differential aerosol property due to coagulation. The last term is an independent source term. The coagulation term introduces a non-linearity, and itself may be expressed as an integral. Coagulation will be detailed in the next section. The solution of the aerosol transport equation requires proper initial and boundary conditions. Because of its nature as a non-linear, integro-differential equation, and due to additional complexity in the initial and boundary conditions, it is often impossible to obtain an analytical solution. The most feasible method of solution is a numerical method.

In order for the aerosol transport equation to be solved numerically, continuous variables (size, space, and time) that are used to express the aerosol property must be discretized. A Eulerian control volume deterministic approach is most commonly used to solve

the transport equation. There are two main mechanisms that change the aerosol property inside a control volume. One is convective flux in/out through the control surfaces, the other is the change in the aerosol property due to coagulation, deposition, condensation, or evaporation. Both mechanisms must coexist in a complete model development of aerosol transport simulation.

Throughout this thesis the coagulation problem will be addressed using the sectional method, in which discrete sections or groups are used to describe a size spectrum. Within each group, the integral average of the aerosol property is assumed constant. The sectional treatment of coagulation may be likened to the multi-group theory for treating particle energies in reactor physics. A collision leads to 'scattering into' a higher size group and 'scattering out' from the initial size group. Because coagulation may change the size spectrum, the choice of size boundaries affects the computational complexity of the coagulation equation. Because coagulation does not contribute to convective flux through the control surfaces, it can be modeled without considering spatial discretization. Therefore, we attempted to model the coagulation mechanism first without spatial discretization and analyze the effects of size sectionalization.

2.3. COAGULATION DYNAMICS

The dynamics of aerosol transport becomes a non-linear, integro-differential equation due to coagulation. Coagulation is assumed here to be a binary collision, which introduces transfer of particles from one size group into another. No de-agglomeration is considered, therefore no "up-scattering" (transfer into smaller groups) is allowed. Because of these characteristics, the simulation of coagulation was first separately studied. The use of a simplifying geometric constraint, its advantages and disadvantages are also discussed in this

section. A coagulation code (SAEROSA) was developed that allows arbitrary sections, and its performance was compared with an existing model (MAEROS) for benchmarking.

2.3.1. Mathematical Representation of Coagulation

In general, the rate of binary coagulation may be computed as an integral quantity of a product among volumes of spheres with radii a and b having a relative velocity with respect to one-another, and their concentrations. The assumption that the particle morphology is spherical allows a significant reduction of computational complexity. The coagulation has a property of a source at a given size group. The coagulation term can be represented as the following integral expression:

$$\left(\frac{\partial n(v,\vec{r},t)}{\partial t}\right)_{coag} = \frac{1}{2}\int_0^v K(u, v-u)n(u,\vec{r},t)n(v-u,\vec{r},t)du - n(v,\vec{r},t)\int_0^\infty K(u,v)n(u,\vec{r},t)du \quad (5)$$

Where, K(u,v) is the collision frequency (also referred as coagulation kernel) between particles with volumes of u, and v.

The coagulation kernel represents the physical process of the collision between two particles. In general, the coagulation is function of aerosol size, position, and time. K(u,v) is often called coagulation kernel, and it represents the physical process of collision between particles with volume u, and v. For example, coagulation kernels due to Brownian motion ($K_B(u,v)$) and gravitational settling ($K_G(u,v)$) are follows:

$$K_B(u,v) = \frac{2kT}{3\mu}\left(2 + \left(\frac{u}{v}\right)^{1/3} + \left(\frac{v}{u}\right)^{1/3}\right) \quad (6)$$

where, k is Boltzmann's constant;
T is temperature of surrounding fluid;
μ is fluid dynamic viscosity;
u, and v are volumes of particles.

$$K_G(u, v) = \frac{\rho g}{6\mu}\left(\frac{3}{4\pi}\right)^{1/3}(v^{2/3} + u^{2/3})\left|v^{2/3}C_v - u^{2/3}C_u\right| \qquad (7)$$

where, ρ is density of particle;
g is gravitational acceleration;
C_v and C_u is Cunningham's correction factor for slip condition.

The rate of change in the aerosol property due to coagulation can be subdivided into two parts: transfer in and out. The first term of equation (5) represents transfer into size v due to a collision between particle size u, and v-u. The second term represents transfer out from size v due to collision between particle size v and everything else. An analytical solution of the above equation is only possible for some simplified cases, for example, when the coagulation kernel is independent of size, and the particle distribution is mono-disperse. The most feasible way to evaluate the coagulation integral is a numerical method. In order to use a numerical method, a discretization of the aerosol size spectrum is first considered.

2.3.2. Aerosol Size Group Discretization

The first step to solve the coagulation equation is the discretization of the aerosol size spectrum into groups. The integral aerosol property in group ℓ, $Q_l(t)$, can be computed by using equation(3) as follows:

$$Q_l(t) = \int_{v_{l-1)}}^{v_l} q(v, t)dv \qquad (3a)$$

where, $v_{\ell-1}$ and v_ℓ are upper and lower size boundary in group ℓ.

In order to derive the discrete coagulation equation, there are three cases that must be considered: 1) aerosol properties added into section ℓ, 2) aerosol properties removed from section ℓ, 3) aerosol properties that remain in section ℓ. Detailed transformation between the continuous and discrete coagulation equation was done by Gelbard and Seinfeld [5]. The

discretized coagulation equation is written as follows:

$$\frac{\partial Q_l}{\partial t} = \frac{1}{2}\sum_{i=1}^{l-1}\sum_{j=1}^{l-1} {}^{1}\beta_{i,j,l} Q_i Q_j - Q_l \sum_{i=1}^{l-1} {}^{2}\beta_{i,l} Q_i - \frac{1}{2}{}^{3}\beta_{l,l} Q_l^2 - Q_l \sum_{i=l+1}^{m} {}^{4}\beta_{i,l} Q_i \qquad (8)$$

The first term represents transfer into group l due to collision of two particular in size groups both smaller than ℓ. The second term is the flux out from group ℓ due to collision between group ℓ and a group smaller than ℓ. The third term gives the flux out from group ℓ due to collisions in the same group. The fourth term is the flux out from group ℓ due to collisions between group ℓ and a group higher than ℓ. The parameters, ${}^{k}\beta$, in each term are the sectional coagulation coefficients, which represent integral values of coagulation kernels between the appropriate group boundaries. Table1 summarizes the ${}^{k}\beta$ values for arbitrary sectionalization (Gelbard[5]). The number of coefficients necessary to calculate the discrete coagulation equation is $\frac{G^3 + 6G^2 - G}{6}$ for an arbitrary discretization of G groups. It is possible to reduce the number of coefficients by careful selection of group boundaries. When the lower (v_{l-1}) and upper boundaries (v_l) of groups meet the condition $v_l \geq 2v_{l-1}$, the first term of equation(8) reduces to single summation. The use of this geometric constraint reduces the number of coefficients to 2G(G+2). The geometric constraint sectionalization allows particle flux into group ℓ only by collision between group ℓ-1 and lower groups. Thus equation (8) may be rewritten as follows:

$$\frac{\partial Q_l}{\partial t} = Q_{l-1}\sum_{i=1}^{l-1} {}^{1}\beta_{i,l-1,l} Q_i - Q_l \sum_{i=1}^{l-1} {}^{2}\beta_{i,j} Q_i - \frac{1}{2}{}^{3}\beta_{l,l} Q_l^2 - Q_l \sum_{i=l+1}^{m} {}^{4}\beta_{i,l} Q_i \qquad (9)$$

Table 2 summarizes the ${}^{k}\beta$ values for the geometric constraint.

Table 1. Inter- and intrasectional coagulation coefficients for arbitrary groups

symbol	conditions	coefficient
${}^{1}\beta_{i,j,\ell}$	$2\le\ell\le m$ $1\le i<\ell$ $1\le j<\ell$ ${}^{1}\beta_{i,j,\ell}={}^{1}\beta_{j,i,\ell}$	$\int_{v_{i-1}}^{v_i}\int_{v_{j-1}}^{v_j}\frac{\theta(v_{l-1}<u+v<v_l)(u+v)K(u,v)}{uv(v_i-v_{i-1})(v_j-v_{j-1})}dudv$
${}^{2}\beta_{i,\ell}$	$2\le\ell\le m$ $i<\ell$ ${}^{2}\beta_{i,\ell}\neq{}^{2}\beta_{\ell,i}$	$\int_{v_{i-1}}^{v_i}\int_{v_{l-1}}^{v_l}\frac{[\theta(u+v>v_l)u-\theta(u+v<v_l)v]K(u,v)}{uv(v_i-v_{i-1})(v_l-v_{l-1})}dudv$
${}^{3}\beta_{\ell,\ell}$	$1\le\ell\le m$	$\int_{v_{l-1}}^{v_l}\int_{v_{l-1}}^{v_l}\frac{\theta(u+v>v_l)uK(u,v)}{uv(v_l-v_{l-1})^2}dudv$
${}^{4}\beta_{i,\ell}$	$1\le\ell<m$ $i>\ell$ ${}^{4}\beta_{i,\ell}\neq{}^{4}\beta_{\ell,i}$	$\int_{v_{i-1}}^{v_i}\int_{v_{l-1}}^{v_l}\frac{uK(u,v)}{uv(v_i-v_{i-1})(v_l-v_{l-1})}dudv$

Table 2. Inter- and intrasectional coagulation coefficients with geometric constraint

symbol	conditions	coefficient
${}^{1}\beta_{i,j,\ell}$	$i<\ell-1$ $j<\ell-1$	0
${}^{1}\beta_{i,\ell-1,\ell}$	$2\le\ell\le m$ $i<\ell-1$	$\int_{v_{i-1}}^{v_i}\int_{v_{l-1}-v}^{v_l}\frac{(u+v)K(u,v)}{uv(v_i-v_{i-1})(v_l-v_{l-1})}dudv$
${}^{1}\beta_{i,\ell-1,\ell}$	$2\le\ell\le m$ $i=\ell-1$	$\int_{v_{i-1}}^{v_i-v_{i-1}}\int_{v_{l-1}-v}^{v_{l-1}}\frac{(u+v)K(u,v)}{uv(v_i-v_{i-1})(v_{l-1}-v_{l-2})}dudv$ $+\int_{v_i-v_{l-1}}^{v_i}\int_{v_{l-2}}^{v_{l-1}}\frac{(u+v)K(u,v)}{uv(v_i-v_{i-1})(v_{l-1}-v_{l-2)}}dudv$
${}^{2}\beta_{i,\ell}$	$2\le\ell\le m$ $i<\ell$	$\int_{v_{i-1}}^{v_i}\int_{v_{l-2}}^{v_{l-1}}\frac{uK(u,v)}{uv(v_i-v_{i-1})(v_{l-1}-v_{l-2})}dudv$ $+\int_{v_{i-1}}^{v_i}\int_{v_{l-1}-v}^{v_l}\frac{vK(u,v)}{uv(v_i-v_{i-1})(v_l-v_{l-1})}dudv$
${}^{3}\beta_{\ell,\ell}$	$1\le\ell\le m$	$\int_{v_{l-1}}^{v_l-v_{l-1}}\int_{v_l-v}^{v_l}\frac{(u+v)K(u,v)}{uv(v_l-v_{l-1})^2}dudv+\int_{v_l-v_{l-1}}^{v_l}\int_{v_{l-1}}^{v_l}\frac{(u+v)K(u,v)}{uv(v_l-v_{l-1})^2}dudv$
${}^{4}\beta_{i,\ell}$	$i\le\ell<m$ $\ell<i$	$\int_{v_{i-1}}^{v_i}\int_{v_{l-1}}^{v_l}\frac{uK(u,v)}{uv(v_i-v_{i-1})(v_l-v_{l-1})}dudv$

2.3.3. Limitation of the Geometric Constraint

The above discussion shows the advantage of the geometric constraint in terms of numerical efficiency, however, it has a trade-off. Using the geometric constraint, it is not possible to resolve narrow distributions or large gradients in size spectra, and the geometric constraint is not suitable for non-lognormal distributions. Since the geometric constraint uses the condition of $v_l \geq 2v_{l-1}$ for the group boundaries, if the size spectrum ranges from v_0 to v_{max}, the maximum number of groups is $G_{max} = \ln\left(\frac{v_{max}}{v_0}\right) / \ln 2$. For each order of magnitude in the particle diameter range, $G_{max}=3(\ln 10/\ln 2)=9.96$. Therefore, there is maximum of nine groups in each order of magnitude of the diameter range. Figure 1 shows a typical mono-disperse aerosol distribution between 0.1 and 5.0μm with a median diameter of 0.5μm and geometric standard deviation of 1.02.

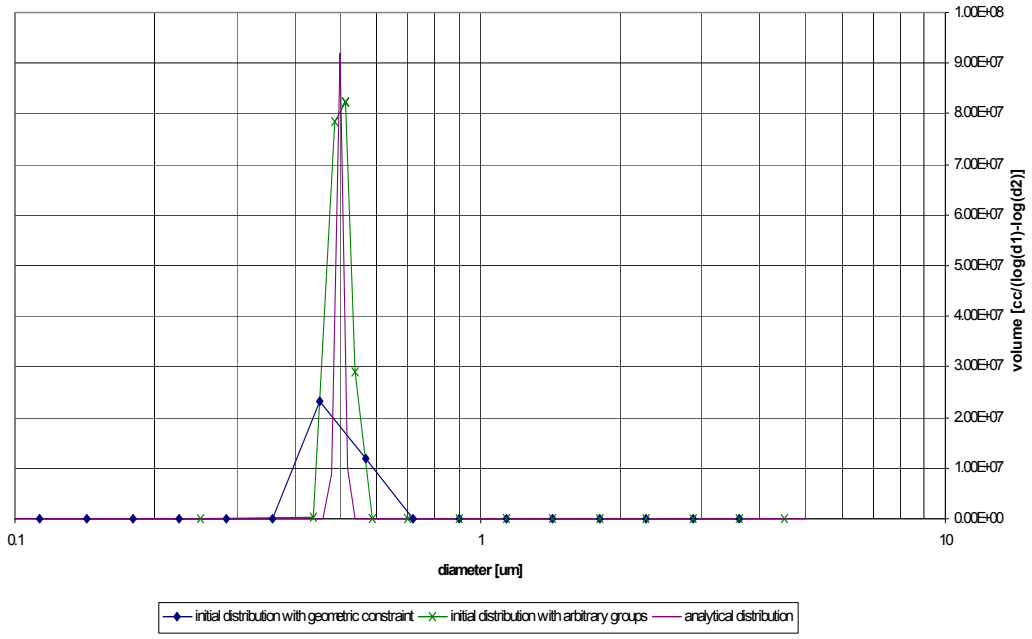

Figure 1. Initial distribution of mono-disperse particles

Here, both the arbitrary sectionalization and the geometric constraint have 16 groups. However, the geometric constraint grouping shows inefficient sectionalization and poor resolution. For narrow distribution, the geometric constraint sectionalization is not very efficient. With the constraint, the maximum number of groups within N standard deviations about the geometric mean diameter, $\left[\frac{d_m}{N\sigma_g} , d_m N\sigma_g \right]$, can be expressed as follows:

$$G_{\max} = 6\ln\left(N\sigma_g\right) \tag{10}$$

where N is number of standard deviations of interest.

In the case of Figure 1 with one standard deviation G_{max} =6ln(1.02)=0.119. Thus, no group boundary can be added within one standard deviation range. If the group boundary around the geometric mean diameter is larger than one standard deviation, the distribution using the geometric constraint will not reproduce the actual distribution correctly. Therefore, for a small geometric standard deviation, a finer separation of group sizes is needed to reproduce the correct distribution. Because of this limitation, the geometric constraint is not always sufficient.

Arbitrary sectionalization is also suitable for a better resolution of both the initial and final size spectrum (after coagulation), regardless of the magnitude of σ_g. Figure 2 shows the initial and final (after 24 hour of coagulation) distribution of atmospheric aerosol by using geometric constraint vs. arbitrary groups as computed by SAEROSA. The SAEROSA code will be discussed in Chapter 3. Atmospheric aerosol is tri-modal with parameters given in table 5. Because the first mode has very small volume, it is not visible in figure 2. The first peak shown in figure 2 is at the median diameter of the accumulation mode with a value of 0.32μm, and the geometric standard deviation of 2.16. It is clear that the size spectrum with geometric constraint after 24 hours of coagulation shows a slight shift to the higher groups. Because of

the coarse group size, especially at larger diameters, the distribution with geometric constraint shows difficulty in reproducing the correct distribution. This tendency becomes more significant when the geometric standard deviation approaches to unity as shown earlier .

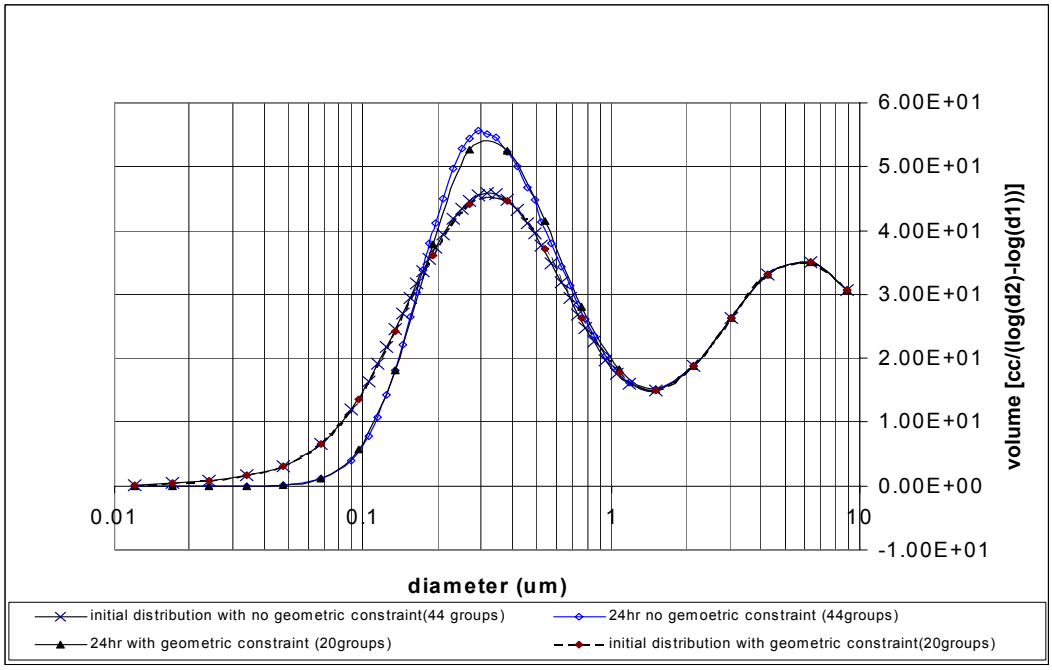

Figure 2. Distribution of atmospheric aerosol by arbitrary grouping and geometric constraint groups

2.3.4. Addition of Coagulation Kernels

Coagulation is due to particle-particle collisions. It occurs when particles have some relative motion. The coagulation kernel K(u,v) has the dimension of $[L^3/T]$, and it represents the volume swept through per unit time by the particle with radius of $r_1 + r_{2,}$ where r_1 and r_2 are the radii of the two particles with volume of u and v. The relative motion of the two particles is usually determined by how the force field acts on both particles. It is not clear whether it is possible to simply add two coagulation kernels to express the resultant of two physical processes. Williams and Loyalka [9] derive an exact expression of coagulation kernels

considering the simultaneous process of Brownian motion and gravitational settling. They also give tabulated values of the deviation of the exact expression from the simple addition. We use these tabulated values to adjust the coagulation kernel when Brownian motion and gravitational settling are simultaneously present.

2.4. DEPOSITION DYNAMICS

Deposition is a removal mechanism in the aerosol transport equation. Without the presence of electrostatic forces, the deposition mechanism is a function of the gravitational acceleration, the material and temperature of the wall, the temperature and humidity of air, and of particle size. Throughout this research, deposition is computed by assuming that the wall is a perfect sink, and that there is no resuspension. Gauss' theorem, as applied to the boundary layer theory, was used to calculate the removal fraction. The rate of change in aerosol property due to deposition may be written as follows:

$$\left.\frac{\partial Q_l}{\partial t}\right|_{deposition} = -R_l Q_l$$

$$R_l^{diffusion} = \frac{A_{wall}}{V} \int_{vl-1}^{vl} \frac{D(v)}{\delta_d(v)}\, dv \qquad (12)$$

$$R_l^{grav} = \frac{A_{floor}}{V} \int_{vl-1}^{vl} V_s(v) dv$$

Where, R_l is removal fraction of group ℓ;
$D(v)$ is diffusion constant of particle with volume v;
$\delta_d(v)$ is diffusion boundary layer of particle with volume v;
$V_s(v)$ is gravitational settling velocity of particle with volume v;
A_{wall} is total area of wall in contact with the aerosol;
A_{floor} is area of floor in contact with the aerosol;
V is volume of computational domain;

In this research, diffusive and gravitational deposition were considered. Diffusion term which appears in equation (4) is important only at close to solid boundary.

2.5. AEROSOL TRANSPORT EQUATION

2.5.1. Discretization of the Computational Domain

In order to model full aerosol transport, in addition to the terms thus far discussed, convective transport must also be included. Convective transport adds a spatial variation in the aerosol property distribution; the flux through control surfaces must be computed to allow communication between control volumes. A rectangular parallelepiped is commonly used for the control volume for simplifying the calculations. If we conserve the integral aerosol property, it is possible to use the following continuity equation:

$$\frac{\partial Q}{\partial t} = \nabla \cdot \vec{J} + Q_{ext} \tag{13}$$

Where $\vec{J}$ is aerosol property current by various mechanisms;

$Q = \sum_{l=1}^{m} Q_l$, is total aerosol property;

Q_{ext} is external source term.

Conservative quantities in aerosol transport are volume and mass distributions. In this research, aerosol property current due to convective motion only is considered. Then, the aerosol property current, $\vec{J}$, can be expressed as $\vec{U}Q$. In this research, the volume distribution is used as aerosol property.

2.5.2. Nodal Method and Computing Flux

The convective term in equation (4) can be rewritten as follows:

$$\nabla \cdot [\vec{U}(v, \vec{r}, t)q(v, \vec{r}, t)] = \vec{U} \cdot \nabla q(v, \vec{r}, t) + q(v, \vec{r}, t)[\nabla \cdot \vec{U}(v, \vec{r}, t)] \tag{14}$$

In low velocities and low velocity gradients, such as those predominant indoors, the second term in RHS of equation (14) is negligible compared to the first term of the RHS. This is equivalent to saying that the divergence term is zero, that is the fluid is incompressible. We assume that fluid is incompressible, the diffusion term only contributes deposition onto solid

boundaries, and the growth term can be neglected. Then equation (4), can be rewritten a in terms of integral aerosol property, Q_l as:

$$\frac{DQ_l(\vec{r},\,t)}{Dt} \;=\; -R_l Q_l(\vec{r},\,t) \;+\; \left(\frac{\partial\, Q_l(\vec{r},\,t)}{\partial\, t}\right)_{coag} \;+\; S_l(\vec{r},\,t) \qquad (4a)$$

The LHS of equation (4a) is the substantial derivative and is equivalent to the continuity equation (13) without the presence of the external source. In order to solve equation (4a), we use a semi-Lagrangian approach, in which the aerosol property is transferred along the streamlines, while the node coordinates are fixed relative to the computational domain. If the integral aerosol property, $Q_l(\boldsymbol{r},t)$, is assumed to be constant inside the control volume, and we write the total aerosol property at node (i, j, k) as ${}_{i,j,k}Q_l$, then equation (4a) in node (i, j, k) can be rewritten as:

$$\frac{d_{i,j,k}Q_l}{dt} \;=\; \sum_{m=1}^{M} {}_{(m\to i,j,k)}^{in}\dot{Q}_l - {}_{i,j,k}^{out}\dot{Q}_l \;-\; R_{l;\,i,j,k}\,Q_l \;+\; \left(\frac{\partial_{i,j,k}Q_l}{\partial\, t}\right)_{coag} + {}_{i,j,k}S_l \qquad (15)$$

where, M is number of nodes connected to node (i, j, k);

${}_{(m\to i,j,k)}^{in}\dot{Q}_l$ is the inward flux to node (i, j, k) from node, m;

${}_{i,j,k}^{out}\dot{Q}_l$ is the outward flux from node (i, j, k).

The outward flux along the streamline at node (i, j, k) with unit node length may be estimated by ${}_{i,j,k}Q\big|_{i,j,k}\vec{V}\big|$, where ${}_{i,j,k}\vec{V}$ is the component-average air velocity vector at node (i, j, k). The previous model (INDASOL3D) [12] used a simple finite difference method to calculate the flux out from node (i, j, k): each velocity component at node (i, j, k) was separately folded into the nodal concentrations. However, it is obvious that the magnitude of a vector quantity is not equal to the scalar sum of the magnitude of components. In the semi-Lagrangian approach, the outward flux can be computed by following method.

In two dimensions, the points that defines the node (i, j) can be expressed as (x_i, y_i), (x_{i+1}, y_i), (x_i, y_{i+1}), and (x_{i+1}, y_{i+1}) as shown in Figure 3.. Within the time interval between t and Δt, the Lagrangian control volume travels by a distance of $\vec{U}\Delta t$. Thus, the points that define the Lagrangian control volume at time t+Δt can be expressed as (x_i+uΔt, y_i+vΔt), (x_{i+1}+uΔt, y_i+vΔt), (x_i+uΔt, y_{i+1}+vΔt), (x_{i+1}+uΔt, y_{i+1}+vΔt). When we integrate the LHS of equation (4a) with respect to time and space, the outward flux from node (i, j) can be computed. First, equation (4a) is integrated with respect to time and it becomes:

$$\int_{V_L}\int_{t}^{t+\Delta t}\frac{DQ_l(\vec{r},t)}{Dt}\,dtdV = \int_{V_L} Q_l(\vec{r}+\vec{U}\Delta t, t+\Delta t)dV - \int_{V_L} Q_l(\vec{r},t)dV \quad (16)$$

where, V_L is the control volume in the Lagrangian system.

At time t, the Lagrangian control volume coincides with the Eulerian control volume. Thus, the second term in the RHS of equation (16) can be written as ${}_{i,j}Q_l(t)$. The first term of the RHS of equation (16) is the outward flux term and can be split among the nodes adjacent to (i, j) into which the aerosol is transported:

$$\begin{aligned}\int_{V_L} Q_l(\vec{r}+\vec{U}\Delta t, t+\Delta t)dV &= \int_{x_i+u\Delta t}^{x_{i+1}+u\Delta t}\int_{y_i+v\Delta t}^{y_{i+1}+v\Delta t} Q_l(\vec{r}+\vec{U}\Delta t, t+\Delta t)dxdy \\ &= \left[\int_{x_i+u\Delta t}^{x_{i+1}} dx + \int_{x_{i+1}}^{x_{i+1}+u\Delta t} dx\right]\left[\int_{y_i+v\Delta t}^{y_{i+1}} dy + \int_{y_{i+1}}^{y_{i+1}+v\Delta t} dy\right] Q_l(\vec{r}+\vec{U}\Delta t, t+\Delta t)\end{aligned} \quad (17)$$

$Q_l(\vec{r}+\vec{U}\Delta t, t+\Delta t)$ is constant in V_L, and can be written as $\frac{{}_{i,j}Q_l}{V_L}$, the nodal average of the aerosol property. Then after performing the multiplications, equation (17) becomes:

$$\int_{V_L} Q_l(\vec{r}+\vec{U}\Delta t, t+\Delta t)dV = {}_{i,j}Q_l\begin{bmatrix}(x_{i+1}-x_i-u\Delta t)(y_{i+1}-y_i-v\Delta t)+(u\Delta t)(v\Delta t)+\\ (u\Delta t)(y_{i+1}-y_i-v\Delta t)+(x_{i+1}-x_i-u\Delta t)(v\Delta t)\end{bmatrix} \quad (18)$$

The first term of the RHS of equation (18) is the aerosol property that remains in node (i, j). The second term of the RHS is the aerosol property that is transferred in node (i+1, j+1). The third and fourth terms in RHS are the aerosol property that is transferred in nodes (i+1, j), and (i, j+1), respectively. Figure 3 shows the flux transfer along the streamline from node (i, j). From figure 3, the fraction of the aerosol property transferred in time Δt, into nodes (i+1, j), (i, j+1), and (i+1, j+1) from node (i, j) is $\frac{|u|\Delta t(ly - |v|\Delta t)}{lxly}$, $\frac{(lx - |u|\Delta t)|v|\Delta t}{lxly}$, and $\frac{|u||v|\Delta t^2}{lxly}$, respectively. Thus, in two dimensional case, the total outward flux term can be expressed as follows:

$$\dot{Q}_{l}^{out}{}_{i,j}\Delta t = Q_{l}{}_{i,j}\,\frac{|u|\Delta t(ly - |v|\Delta t) + (lx - |u|\Delta t)|v|\Delta t + |u||v|\Delta t^2}{lxly} \tag{19}$$

It is easy to generalize into three dimensional case. Table 3 shows the amount of aerosol property transfer from node (i, j, k) to adjacent nodes. Δt in table 3 is the time step of each iteration. In order to avoid unrealistic conditions, the amount of aerosol property transferred from node (i, j, k) in one time step must be smaller than that of the existing amount in node (i, j, k). Thus, the quantity inside the bracket of the last row of table 3 must be smaller than $lx \times ly \times lz$. By using this condition, the time step of each iteration can be computed adaptively. Since a small time step introduces more numerical diffusion, it is important that an efficient time step should be computed adaptively.

Inward and outward flux terms in equation (15) can be calculated from table 3. A fully implicit method was used to solve equation (15). In equation (15), the coagulation and the independent source term depend only on the node property, and the magnitude of the coagulation term is often small compared to the convective term. The coagulation term also

introduces a non-linearity into the equation, and makes the convergence slower. Therefore, the coagulation term is treated as source term whose value is updated in an outer iteration.

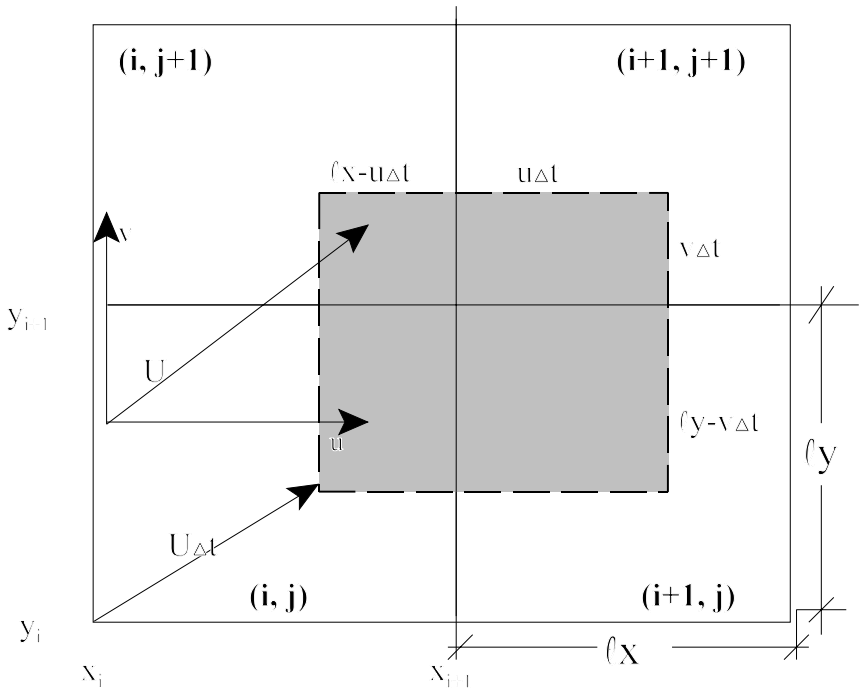

Figure 3. Flux transfer along streamline in 2-D case.

Table 3. Amount of aerosol property transferred into various nodes from node (i,j,k).

node aerosol property transferred to	amount of aerosol property transferred
$(i \pm 1, j, k)$	$\frac{Q(\lvert u\rvert \Delta t)(ly - \lvert v\rvert \Delta t)(lz - \lvert w\rvert \Delta t)}{(lx)(ly)(lz)}$
$(i, j \pm 1, k)$	$\frac{Q(lx - \lvert u\rvert \Delta t)(\lvert v\rvert \Delta t)(lz - \lvert w\rvert \Delta t)}{(lx)(ly)(lz)}$
$(i, j, k \pm 1)$	$\frac{Q(lx - \lvert u\rvert \Delta t)(ly - \lvert v\rvert \Delta t)(\lvert w\rvert \Delta t)}{(lx)(ly)(lz)}$
$(i \pm 1, j \pm 1, k)$	$\frac{Q(\lvert u\rvert \Delta t)(\lvert v\rvert \Delta t)(lz - \lvert w\rvert \Delta t)}{(lx)(ly)(lz)}$
$(i \pm 1, j \pm 1, k)$	$\frac{Q(\lvert u\rvert \Delta t)(ly - \lvert v\rvert \Delta t)(\lvert w\rvert \Delta t)}{(lx)(ly)(lz)}$
$(i, j \pm 1, k \pm 1)$	$\frac{Q(lx - \lvert u\rvert \Delta t)(\lvert v\rvert \Delta t)(\lvert w\rvert \Delta t)}{(lx)(ly)(lz)}$
$(i \pm 1, j \pm 1, k \pm 1)$	$\frac{Q(\lvert u\rvert \Delta t)(\lvert v\rvert \Delta t)(\lvert w\rvert \Delta t)}{(lx)(ly)(lz)}$
Total aerosol property leaving from node (i,j,k)	$\frac{Q}{(lx)(ly)(lz)}\left[\begin{array}{l} uvw(\Delta t)^3 + u(\Delta t)lylz + v(\Delta t)lxlz + w(\Delta t)lxly \\ - uv(\Delta t)^2 lz - uw(\Delta t)^2 ly - vw(\Delta t)^2 lx \end{array}\right]$

CHAPTER 3. SIMULATION OF COAGULATION AND DEPOSITION: THE SAEROSA CODE

3.1. INTRODUCTION

Aerosol size range of interest spans several orders of magnitude. Coagulation and deposition mechanisms are largely affected by its size. Validation of a coagulation mechanism alone is very difficult because 1) the experimental results must be very precise, 2) of the nature of the hypothetical initial condition (a well-mixed hypothesis), and 3) a separation of each physical process is nearly impossible. In this chapter, a coagulation model 'SAEROSA' and its benchmarking against MAEROS [13] are described. Two initial conditions were used in order to analyze the code's capabilities for all size ranges, and time scales. One is atmospheric aerosols time evolution. This was done to benchmark the applicability in low concentration, smaller aerosol size, and long time scale. The second is pipe scale particle simulation. This is done to benchmark the applicability in high concentration larger aerosol size, and short time scale.

3.2. MODEL DESCRIPTION

Our developed model, SAEROSA, was benchmarked against MAEROS [13]. Both SAEROSA and MAEROS predict aerosol size spectrum inside a homogeneous mixture. SAEROSA was developed based on the formulations given in Chapter 2. Table 4 shows a summary of model capabilities of SAEROSA and MAEROS. In order to benchmark SAEROSA against MAEROS, 20 groups with geometric constraint were used for size discretization. Results of coagulation only, then coagulation and deposition simulations were quantitatively compared.

Table 4. Model comparison between SAEROSA and MAEROS

NAME		SAEROSA	MAEROS
Capability	Coagulation	YES	YES
	Deposition	YES	YES
	Condensation, Evaporation	NO	YES
	Species	Single Species	Multi-Species
Aerosol Property		Volume Concentration	Mass Concentration
Group Structure		Arbitrary	Geometric Constraint
	Number of group	50 group max	20 group max
Numerical Method		Runge-Kutta Verner $5,6^{th}$ order	Runge-Kutta Fehlberg $4,5^{th}$ order
Computational Time	(for 24 hour simulations with 20 groups)	~1 min	~1 min

3.3. BENCHMARK 1: ATMOSPHERIC AEROSOL TIME EVOLUTION

The simulation of atmospheric aerosol was first benchmarked. Physical processes included in this computation are coagulation due to Brownian motion and gravitational settling, and deposition due to gravitational settling. Atmospheric aerosols have tri-modal distribution, with nucleation, accumulation, and coarse modes. The nucleation mode consists of particles with diameter of less than 0.1μm. The accumulation mode includes particles with a diameter between 0.1 to 2.0μm. Coarse mode particles have a diameter greater than 2.0μm. Seigneur and Seinfeld [4] show parameters of atmospheric aerosol distribution for conditions of clear, hazy and urban atmospheres. In this section, the parameters for urban atmosphere were used. Table 5 shows the parameters of atmospheric aerosols in urban environment. These parameters were used as initial conditions for the benchmark simulation. Figure 3 shows the 24 hour time

evolution due to coagulation only, and figure 4 shows 24 hour time evolution due to coagulation and deposition as computed by SAEROSA and MAEROS.

Figure 4 and 5 show a good agreement between the MAEROS and SAEROSA simulations. For the simulation with coagulation only, the relative error, $\frac{{}^{24hr}_{MAEROS}Q_l - {}^{24hr}_{SAEROSA}Q_l}{{}^{24hr}_{MAEROS}Q_l} \times 100$, in the nucleation mode is about 5~110%, while in the accumulation and coarse mode is less than 2.5%. The reason for the apparently high relative discrepancy in the nucleation mode is that the fractional loss during 24 hr is up to 10^{12}. Because of the high collision frequency, a very low amount of aerosol property is left in the nucleation size groups (less than one particle per group bin), thus the statistical error in this size range gives a high apparent discrepancy between the two simulation results. In the simulation of both coagulation and gravitational deposition, the ranges of the relative discrepancies in nucleation, accumulation, and coarse modes are 3~45%, 1~7%, and 30~1000%, respectively. The discrepancies in fractional loss are less than 3% in the entire distribution. There is very high apparent relative discrepancy in coarse mode. In this mode, most particles are deposited by gravitational settling, and this range of the spectrum has less than one particle left in the group bins. In accumulation mode, the peak predicted by SAEROSA is slightly shifted to the higher size range than that of MAEROS. This is due to the different methods that are used to summing the coagulation kernels in the two codes. While MAEROS uses a simple addition of the kernels, SAEROSA utilizes more sophisticated method. Williams [9] shows a relationship between the exact kernel of simultaneous Brownian and gravitational coagulations and that of simple addition as:

$$K^{B+G}_{exact}(u, v) = \gamma \; K^{B+G}_{simple}(u, v) \tag{20}$$

The factor γ ranges from 1.0 to 1.3. Coagulation of particles in accumulation mode has the highest value of γ. Thus, the result of SAEROSA gives a slight shift to the higher groups. Throughout this simulation, the absolute discrepancy is less than 1.0[$\mu m^3/cc$] . Despite the apparent discrepancies the group with very low concentration, SAEROSA reproduces the MAEROS results remarkably. This concludes the benchmarking SAEROSA against MAEROS for low concentration, small sizes and long time scales.

Table 5. Parameters of atmospheric aerosols in urban environment

Parameter	Nucleation	Accumulation	Coarse
Median Diameter [μm]	0.038	0.32	5.7
Geometric Standard Deviation	1.8	2.16	2.21
Total Volume [cc/cc]	0.63e-12	0.384e-10	0.308e-10

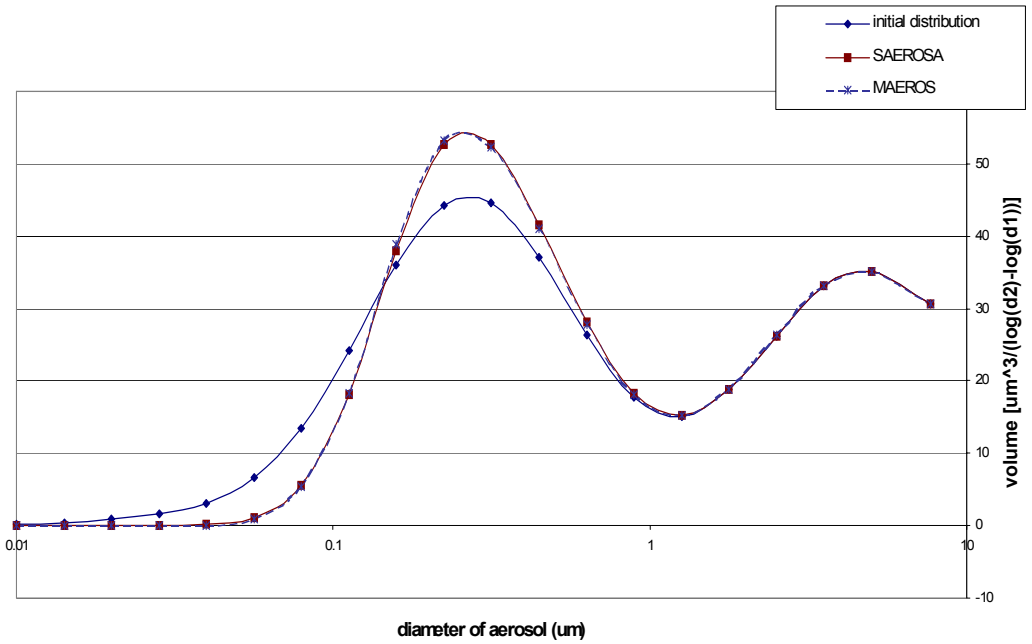

Figure 4. Urban aerosol 24 hour time evolution due to coagulation

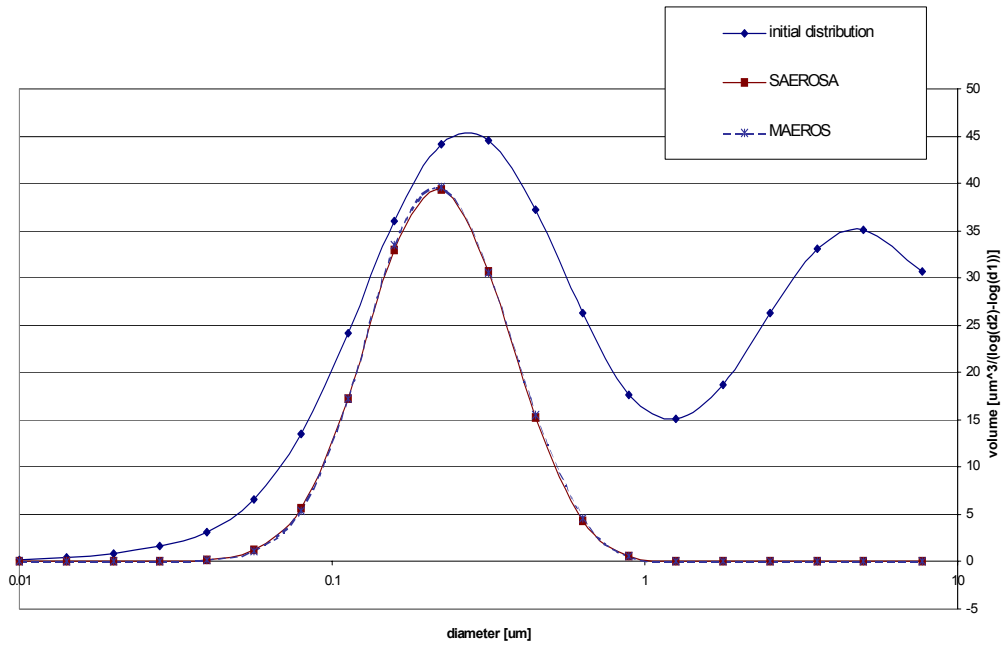

Figure 5. Atmospheric aerosol 24 hour time evolution due to coagulation and deposition

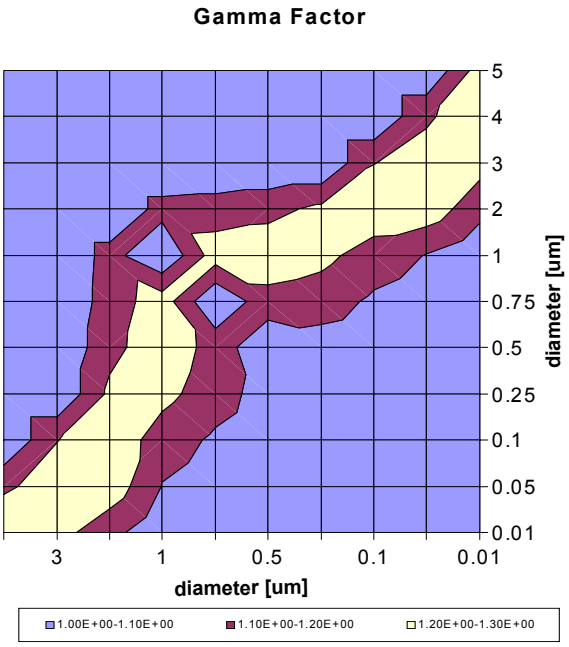

Figure 6. Gamma factor in equation (20) as function of diameter of aerosol

3.4. BENCHMARK 2: SIMULATION OF PIPESCALE PARTICLES

Atmospheric aerosol has a tri-modal distribution with a relatively low concentration throughout the spectrum, and with most of the particles in the first mode. Thus, the time scale of the simulation is long (relaxation time $\geq$1 day). In order for our code to be tested for the entire aerosol size range and time scale of interest, a higher concentration aerosol with relatively large particles undergoing rapid changes in size should also be considered. In this benchmark, we have simulated the aerosol size spectrum evolution of pipe scale particles whose geometric mean diameter is 50μm. Additional parameters are listed in Table 6. Pipe scale particles are generated during pipe cleaning in the oil industry, and since radon and radon daughters may be attached to those particles, their behavior is of interest to the Health Physicist.

60 and 300seconds simulations were performed using SAEROSA, and benchmarked against MAEROS. Figures 7 and 8 show the results of the simulations. Relative discrepancies of both 60 seconds and 300 seconds simulations are less than 35% in all ranges with number of particles greater than one. Relative discrepancy in aerosol property left in 60 seconds is 0.8%, and that in 300 seconds is 8.8%.

Table 6. Parameters of pipescale particle distribution function.

	Pipe scale particles
Geometric mean diameter	50μm
Geometric standard deviation	3.0
Volume concentration	1.0235E-4 [cc/cc]
Density of particles	2.0 [g/cc]

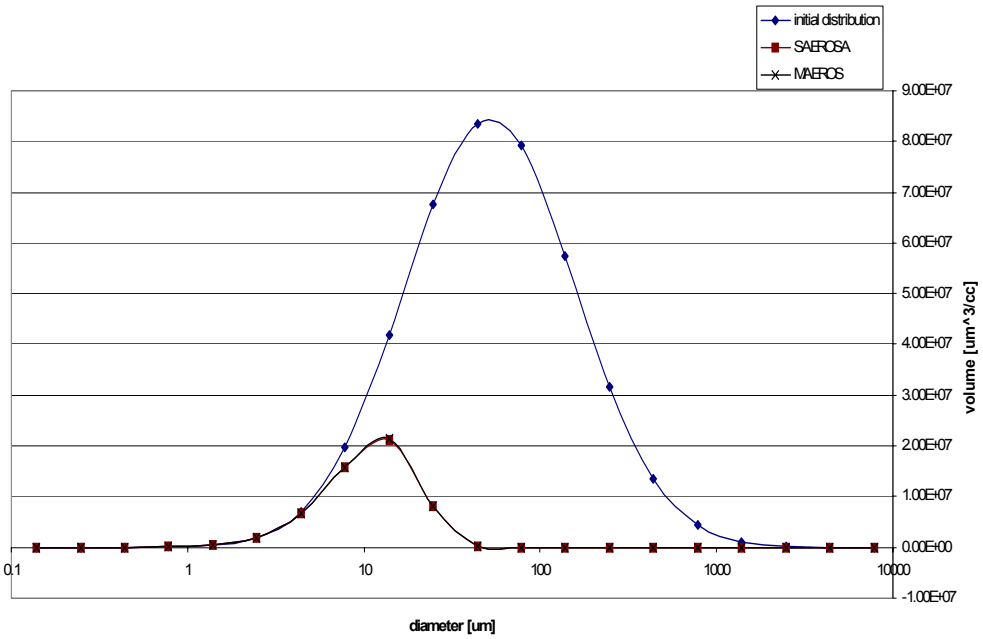

Figure 7. Pipescale particles simulations with 60 seconds

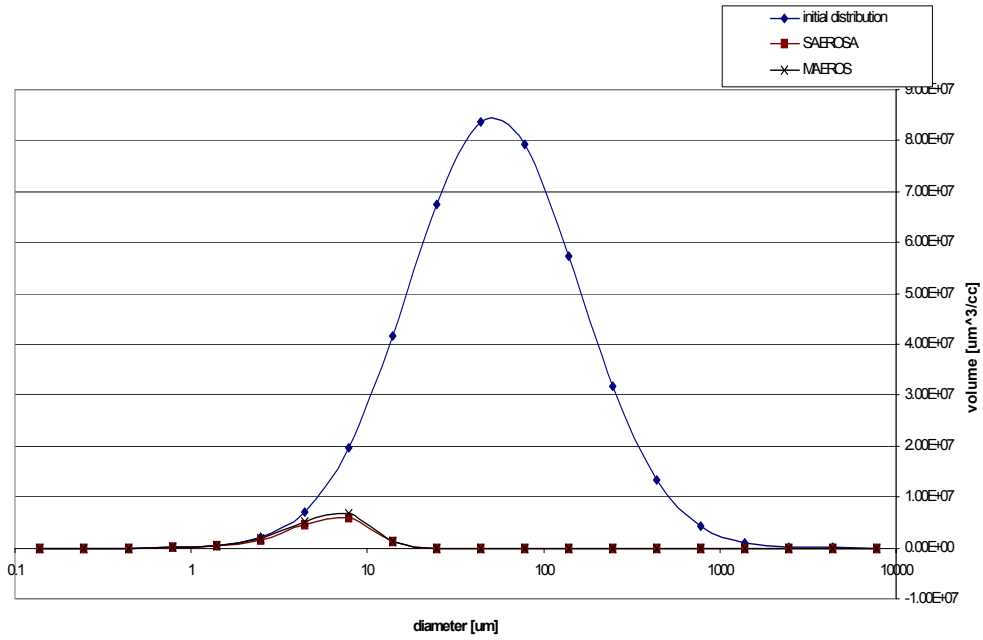

Figure 8. Pipescale particles simulations with 300 seconds.

CHAPTER 4. SPATIAL AND TEMPORAL SIMULATION OF AEROSOL TRANSPORT IN THE ENVIRONMENTAL CHAMBER: THE CAEROT CODE

4.1. INTRODUCTION

The previous chapter shows the validity of the developed coagulation/deposition code, SAEROSA. This code does not consider spatial variation. It assumes that the aerosol is homogeneously distributed in the volume of interest. Spatial distribution is, however, very important in various applications. A new code, CAEROT, was developed which incorporates features of SAEROSA, and introduces the spatial variation of the aerosol property. In this chapter, the simulation of the spatial and temporal evolution of aerosol and its validation against the experimental results are discussed. Experiments were done in the Aerosol Lab at the LSU Nuclear Science Center by Sajo and Raja [12]. A previous code developed by Sajo and Raja (INDASOL3D) had difficulty predicting the correct peak magnitude and tended to diverge at long simulation times. The current code (CAEROT) includes advanced nodal methods, time dependent particle sampling and release mechanisms for better peak prediction and numerical efficiency. An external Computational Fluid Dynamics(CFD) code was used to compute the fluid velocity profile in the experimental aerosol chamber. This was saved as an input data file to CAEROT. The velocity sensitivity of the code is also discussed here.

4.2. MODEL DESCRIPTION, PROBLEM SETUP

The CAEROT code computes the space and time dependent aerosol size spectrum by using the Eulerian control volume finite difference approach. An external CFD code is needed to compute the velocity field inside the computational domain. In this research, the Fire

Dynamics Simulator 3.0 (FDS3), developed by the National Institute of Standards and Technology (NIST) was used as the external CFD code because it was specifically developed to simulate air flow in enclosed atmospheres. The node averaged velocity was used as the velocity profile. Coagulation, deposition, convective transport, time dependent source, and time dependent sampling of particles are included in the CAEROT code. Table 7 shows the model description summary of CAEROT.

Table 7. CAEROT description

	Name	CAEROT
Aerosol Physics	Convection	No-Slip, Fluid Driven
	Deposition	Diffusive, and Gravitational
	Coagulation	Brownian, and Gravitational, Slip Enabled
	Source	Space and Time Dependent
	Particle Sampling	Space and Time Dependent
Discretization	Size Group	Arbitrary Groups
	Spatial Grid	Uniform Rectangular Cartesian
	Time Step	Adaptive with maximum step specified

For code validation, experimental results obtained by Sajo and Raja [12] were used . In this thesis only one of these experiments is compared to the computational results. The physical dimensions of the environmental chamber is 180x60x150cm. The aerosol release location for the experiment used here was (60, 30, 40) cm, and the sampling location is (110, 30, 83) cm. In the experiments, a PG-100 nebulizer and LASAIR 510 optical particle counter manufactured by Particle Measuring Systems (PMS) were used for particle release and sampling, respectively. NIST traceable 0.5 μm particle were used as source. The schematics of the geometry is shown in Figure 9, while table 8 shows the experimental parameters used for simulation.

Table 8. Experimental parameters of environmental chamber simulation.

Physical Dimension	180x60x150cm^3
Aerosol Release Location	x=60, y=30, z=40cm
Aerosol Sampling Location	x=110, y=30, z=83cm
Total Volume of Particles Released	3.518586E-6 [cc]
Aerosol Release Duration	60 [seconds]
Air Sampling Flux	1.0 [Liter/min]
Median Diameter of Source Aerosol	0.5 [μm]
Geometric Standard Deviation	1.018928

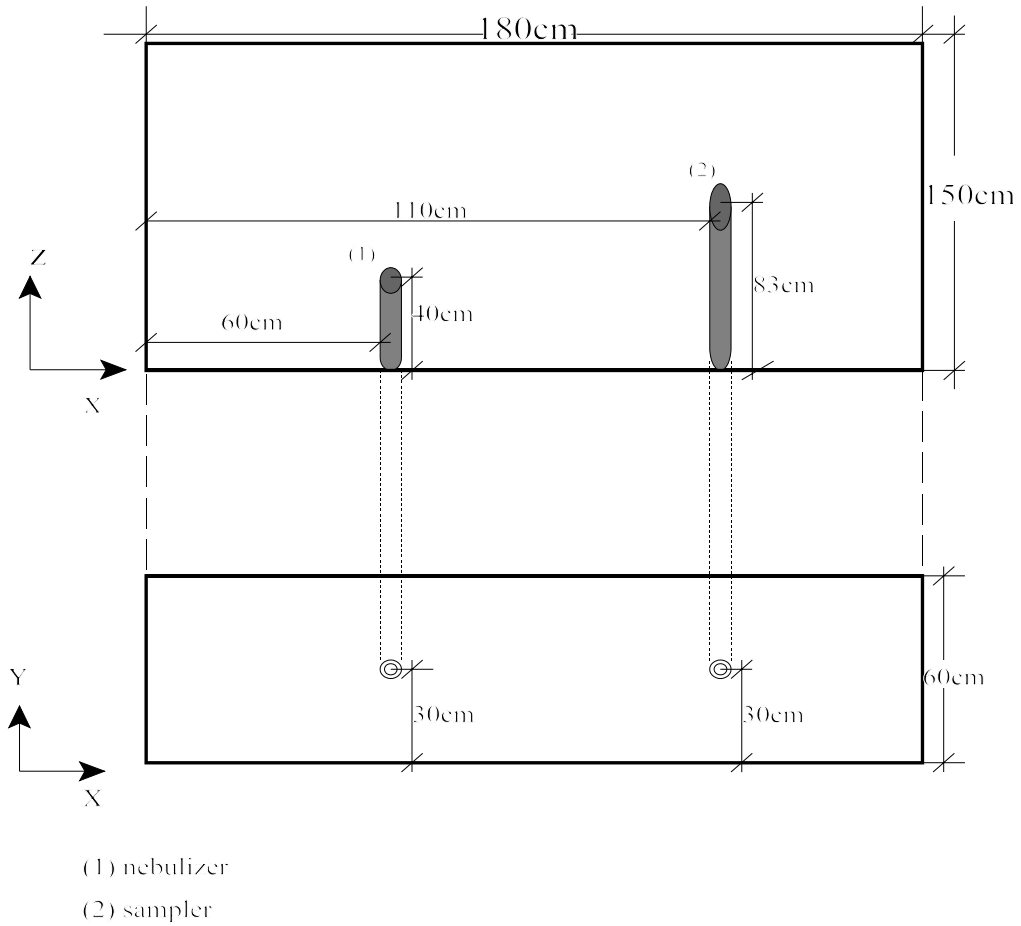

Figure 9. Schematic design of environmental chamber

4.3. SIMULATION RESULTS

Two simulations with different node sizes were done. The first simulation used the node size of 10x10x10 cm, with 1620 total nodes. The second simulation used 5x5x5 cm node size with 12960 total nodes. 12 minutes of aerosol time evolution was simulated. The average computational time for 10x10x10 nodes was about 7 minutes and 4 minutes in Unix platform for the 20 and 5 size groups, respectively. The average computational time for the 5x5x5 cm node size was about 3 hours and 1 hour in Unix platform for 20 and 5 size groups, respectively. Figure shows the simulation result of INDASOL3D and its comparison against the experimental data. Figures 10 and 11 show the simulation results using CAEROT with node sizes of 10x10x10, and 5x5x5cm, and its comparison against experimental data.

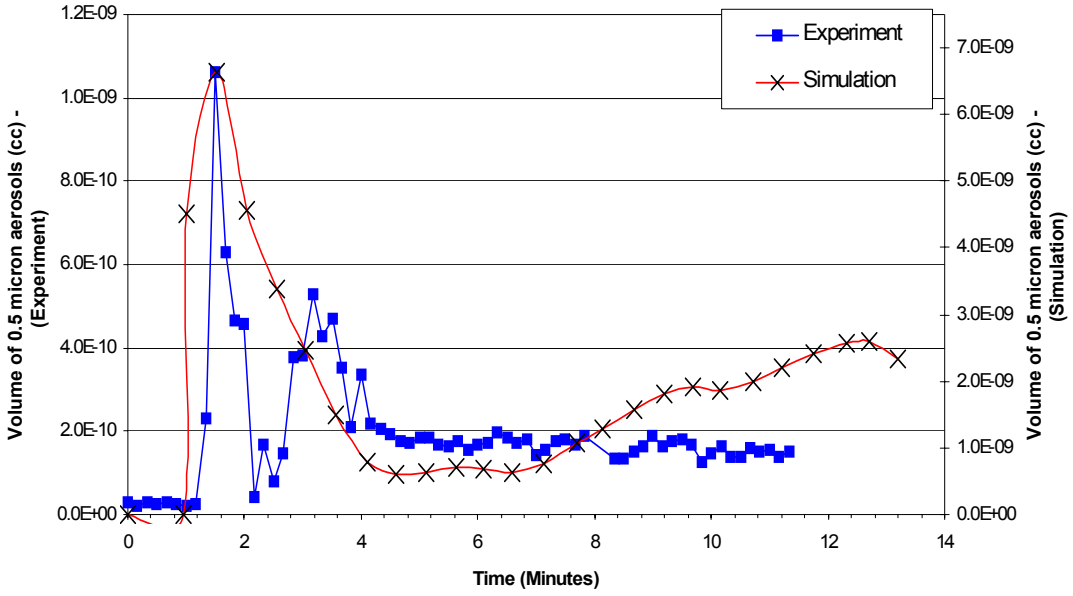

Figure 10. INDASOL3D simulation with 10x10x10cm node size

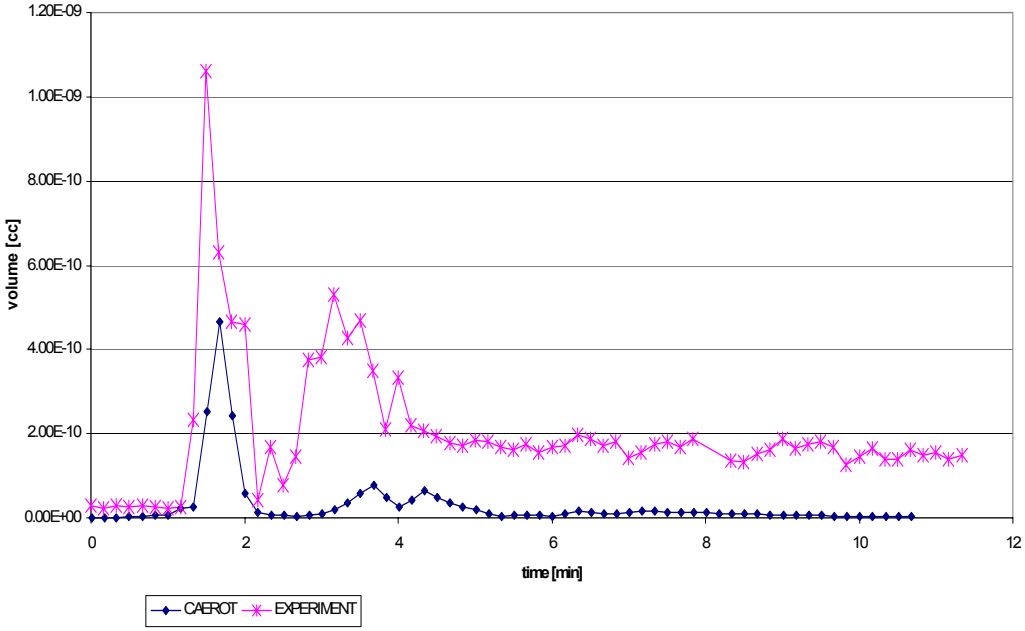

Figure 11. CAEROT simulation result with 10x10x10cm node size

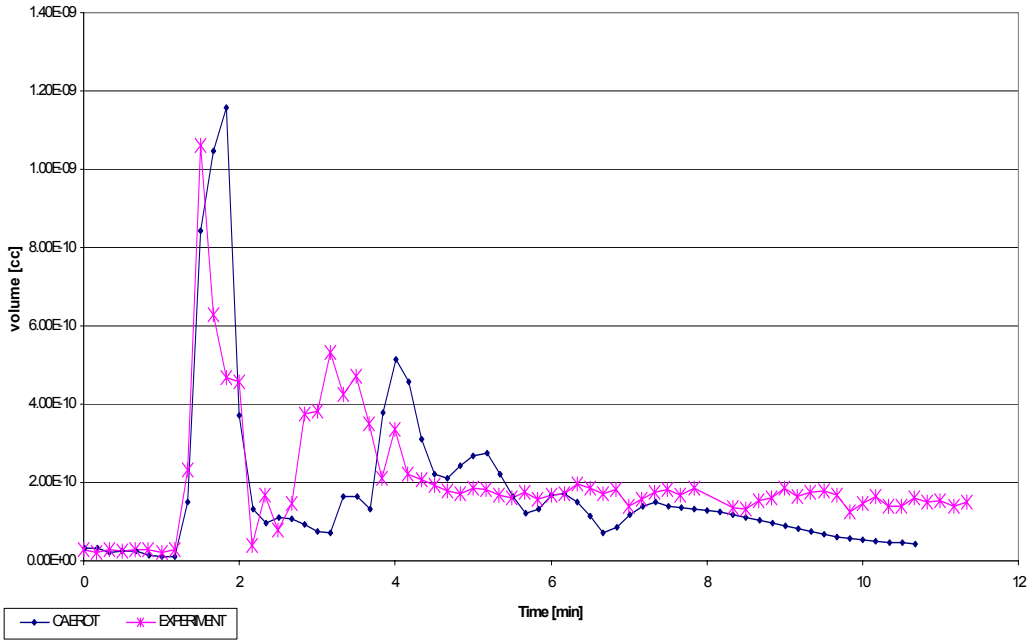

Figure 12. CAEROT simulation result with 5x5x5cm node size

The INDASOL3D results in figure 10 show a quantitative error of about a factor of 5 at the first peak, and show the divergence after 8 minutes. The second experimental peak appears to be interpolated with the first one. It must be noted that the INDASOL3D code does not have the time dependent sampling mechanism implemented , and its time resolution is one minute. The actual values plotted in Figure 10 are the concentrations of the node that corresponds to the position of the intake tube.

The CAEROT results in figure 11 show a quantitative error of about a factor of 2 at the first peak. It also shows that the second peak is resolved. The quantitative error is due to the computational simulation of the sampling mechanism. Since the sampling mechanism collects particles from one node that corresponds to the sampling location, the averaged concentration at the node of the sampler is less than that of the localized sample point.

The CAEROT results using a finer mesh, in figure 12, show a good agreement in the first peak in both time and magnitude, and it is able to resolve the second peak with good agreement in magnitude. The relative discrepancies in Figure 12 at the peaks are 10% and 3% for the first and the second peak, respectively. The simulation of the first peak shows a delay of 20 seconds. This delay is due to the difficulty in the synchronization of the CFD code and the CAEROT code. Figure 12 also shows 50 seconds shift in the prediction of the second peak. The delay of the second peak is due to the difficulty in the velocity computation at very low velocity. CAEROT tracks numerical diffusion by observing the aerosol property conservation for the simulation. Table 9 summarizes the fractional property concentration by time.

Throughout the development of the code, one of the biggest problems is resolving low velocities. The FDS3 simulation gives velocities of about ~1[mm/sec] after the nebulizer is

turned off. However, actual scalar velocity measurements yielded ~1[cm/sec] everywhere in the chamber. In this range of the velocity, the stochastic events driven by small changes in the environmental parameters, such as local temperature or pressure fluctuations, dominate the generation of the air velocity. Thus, it is very difficult to reproduce the exact velocity field. The shifts in the second peak of Figure 12 is a consequence of this mismatch in the low velocity field. In this range of flow regime, transport due to diffusion might not be negligible. Apart from deposition, the CAEROT code does not take into account diffusive transport. When the magnitude of the convective transport becomes comparable to that of other transport mechanisms, the code will have to include all of the aerosol physics for better prediction.

Table 9. The aerosol property conservation in the simulation

	10x10x10cm node	5x5x5cm node
Time (min)	$\frac{Q(t) - Q(0)}{Q(0)}$	$\frac{Q(t) - Q(0)}{Q(0)}$
1.0	2.62E-5	3.72E-6
3.0	3.00E-5	3.44E-6
5.0	3.06E-5	1.84E-4
7.0	3.17E-5	5.90E-3
9.0	3.16E-5	1.30E-2
12.0	3.48E-5	1.76E-2

CHAPTER 5. CONCLUSIONS, AND RECOMMENDATIONS FOR FURTHER WORK

5.1. CONCLUSION

A 3-D aerosol transport simulation and validation was done in this research. Three steps were taken for this project: 1) Mathematical model development of aerosol transport, 2) Coagulation/deposition simulation in a well-mixed chamber, 3) Numerical aerosol transport simulation including convective transport and coagulation. In the mathematical model development, the advantages and the disadvantages of the specific group sectionalization were analyzed in terms of numerical efficiency and resolution. It is found that geometric constraint sectionalization reduces computational cost with the trade off of spectrum resolution. We conclude that for a narrow distribution (i.e. small geometric standard deviation), arbitrary sectionalization gives a flexibility, which with carefully selected group boundaries gives good numerical efficiency as well. Arbitrary sectionalization will be also suitable for non-lognormal distributions.

The Coagulation/Deposition model (SAEROSA) was benchmarked against the existing code (MAEROS). The codes showed very good agreement in the case of both small and large time scale simulations. Large relative discrepancies were observed at very low concentrations (<1[particle/group]). This discrepancy is unavoidable due to different numerical schemes and round-off error, but its significance is marginal, if any.

The full physics transport model (CAEROT) was developed and validated against experimental data. New numerical methods and mechanism were developed. The simulation results were greatly improved from the results of INDASOL3D. However, there exists a

difficulty in the generation of low velocity field using an external CFD code. Dependence on the external CFD code is still significant.

5.2. RECOMMENDATION

The velocity field of the experiment that is used for validating CAEROT is transient. The velocity profile used in the simulation was updated in 10 seconds interval. Better results can be expected when the external CFD code can be embedded into CAEROT, or vice-versa, so that "real-time" velocity data can be used.

The spatial homogenization process in the experiment seems much faster, and it results in a slower decay in the sampled aerosol property than in the simulations. This can be improved when the turbulent and Brownian diffusions are included in the code. It might be necessary to change the numerical method when the dominant mechanism of convective transport changes.

REFERENCES

[1] N. Fuchs (1964) The Mechanics of Aerosol, Pergamon Press, New York

[2] M.M.R. Williams, and S.K. Loyalka (1991) Aerosol Science: Theory and Practice, Pergamon press.

[3] M. Sitarski and J.H. Seinfeld (1977) "Brownian coagulation in the transition regime", Journal of computational physics, Vol.28, pp. 357-375

[4] Seigneur et al (1986), "Simulation of Aerosol Dynamics: A Comparative Review of Mathematical Models", Aerosol Science and Technology, Vol. 5, pp.205-222

[5] F. Gelbard, Tambour, and J.H. Seinfeld (1980), "Sectional Representation for Simulating Aerosol Dynamics", Journal of Colloid and Interface Science, Vol. 76, No.2, pp541-556

[6] Lai, and Nazaroff (2000), "Modeling of Indoor Particle Deposition from Turbulent Flow onto Smooth Surfaces", Journal of Aerosol Science, Vol.31(4) pp. 463-476

[7] C. N. Davies, (1966), "Brownian Deposition of Aerosol Particles from Turbulent Flow Through Pipes", Mathematical and Physical Sciences, Vol.290, Issue 1423 pp. 557-562

[8] R. Tsai, and L.J. Liang, (2001), "Correlation for Thermophoretic Deposition of Aerosol Particles onto Cold Plate", Journal of Aerosol Science, Vol.32 (4) pp.473-487

[9] E. Sajo, H. Zhu, and J.C. Courtney (2002), "Spatial Distribution of Indoor Aerosol Deposition under Accidental Release Conditions", Health Physics, Vol.83 (6), pp 871-883, (2002)

[10] J.J Whicker, et al (2001), "Influence of Room Geometry and Ventilation Rate on Airflow and Aerosol Dispersion: Implications for Worker Protection",Health Physics, Vol.82 (1), pp. 52-63

[11]J.J. Whicker, et al (1997), "Evaluation of Continuous Air Monitor Placement in a Plutonium Facility", Health Physics, Vol.72 (5), pp.734-743

[12] S. Raja, (2001) "Simulation and Benchmarking of Aerosol Transport in Confined Spaces", Thesis, Louisiana State University

[13] F. Gelbard, RSICC Peripheral Shielding Routine Collection MAEROS, contributed by Sandia National Laboratories, Albuquerque, New Mexico, Oak Ridge National Laboratory, RSICC Code Package PSR-466, (1982)

APPENDIX: INPUT FILE FORMATS

A.1. INTRODUCTION

The first step to run SAEROSA and CAEROT is to set up text input files. Both programs are made available as single load modules. To run SAEROSA, type at the command type at the command like $saerosa *input*.in. Likewise, to run CAEROT, type the command like $caerot *input*.in. The input files are organized into slots or arrays. Each array of the input file starts with a character string and is followed by the corresponding values. Corresponding values must be written as a separate record from a character string. From the third array on, the order of the arrays is not restricted. The input file formats for both SAEROSA and CAEROT are described here.

A.2. SAEROSA SAMPLE INPUT FILE AND DESCRIPTION

A.2.1. Sample Input File

```
urban_2
group
2
20
0.01, 0.01413, 0.01995, 0.02818, 0.03981, 0.05623, 0.07943, 0.1122, 0.1585, 0.2239, 0.3162,
0.4467, 0.6310, 0.8913, 1.259, 1.778, 2.512, 3.548, 5.012, 7.708, 10.00

dist
1
3
0.038, 0.63e-12, 1.80
0.320, 38.4e-12, 2.16
5.700, 30.8e-12, 2.21

time
3600.0

coag
```

```
1
depo
1
temp
300.
dens
1.0

volu
1.5e6
area
6.0e4, 1.0e4
end
```

A.2.2 Input File Description

1st array: *title* (Required)

"urban_2" -The first array is a character string that corresponds to the title of the simulation. "Title" is used to name the output file ("title.out")

2nd array: *group sectionalization* (Required)

"group" -Character string "group" is used for indicating that the following sequence of numbers is used for sectionalization.

cstraint -Integer value that determines whether the size group structure uses geometric constraint or not. This integer value can only be 1 or 2.

cstraint =1 - Geometric constraint will be used for group sectionalization. Two values must follow: minimum and maximum diameters of interest in terms of [μm] (*dmin, dmax*) written as a separate record.

cstraint =2 -User specified arbitrary sections will be used. The following value on the next record is the number of groups (*ign*), and should be an integer. Then in a separate record, ign+1 real values must

follows, representing the group boundaries in terms of [μm].

3rd array: *initial distribution of aerosol* (Required)

"dist" -Character string "dist" is used for indicating that the next array of numbers is for the initial distribution of the aerosol.

dist_type -Integer value that determines whether the initial size distribution is log-normal or a user-specified arbitrary initial distribution. This integer value can only be 1 or 2.

dist_type =1 -Log-normal distribution is used as initial distribution. Following this as a separate record, the integer value of number of modes (*N_mode*) must be specified. Then, N_mode sets of real triplets follow which describe the median diameter (*m_dia*) in [μm], the volume concentration (*t_vol*) in [cc/cc], and geometric standard deviation (*stdev*) in this order. Each triplets value must be written as a separate record.

dist_type=2 -User specified distribution is used for initial distribution. This is followed by an array of values giving the volume concentration in each group (*qtot(l)*) in [cc/cc]. These should be real values and start from the smallest groups. An array of *qtot(l)* must be written as a separate record from *dist_type*.

4th array: *simulation time* (Required)

"time" -Character string "time" is used for indicating that the following value is simulation time.

sim_time -This real value specifies simulation time in terms of [sec].

5th array: *coagulation type* (Optional)

"coag" -Character string "coag" is used for indicating that the following value determines the coagulation type

coag_type -This integer value specifies the type of coagulation. The value should be 1, 2, or 3. Default value is 1.

coag_type=1 -Brownian motion and Gravitational settling are considered for coagulation. Tabulated values of the relationship between the simple addition of two kernels and the exact expression of simultaneous Brownian and gravitational coagulation are used from [2].

coag_type=2 -Only Brownian motion is considered.

coag_type=3 -Only gravitational coagulation is considered.

6th array: *deposition model* (Optional)

"depo" -Character string "depo" is used for indicating that the following value determines the deposition type.

dep_type -This integer value specifies the type of deposition. The value must be 1, 2, or 3. Default value is 1.

dep_type=1 -Simultaneous Brownian and gravitational deposition are considered.

dep_type=2 -Only Brownian deposition is considered.

dep_type=3 -Only gravitational deposition is considered.

7th array: *temperature of air* (Optional)

"temp" -Character string "temp" is used for indicating that the following value is the temperature of air in which aerosol coagulation takes place.

t -This real value specifies the temperature of air in terms of K. Default value is 300 K.

8th array: *density of particles* (Optional)

"dens" -Character string "dens" is used for indicating that the following value is the density of aerosol particles.

dens -This real value specifies the density of particle in terms of [g/cc]. Default value is 1.0 [g/cc]

9th array: *volume of chamber* (Optional)

"volu" -Character string "volu" is used for indicating that the following value is the volume of chamber or the coagulation domain.

volume - This real value specifies the volume of chamber in terms of [cc]. Default value is 1E6 [cc].

10th array: *area of enclosing walls* (Optional)

"area" -Character string "area" is used for indicating that the following values specify the areas of the wall and floor.

area, floor -Two real values are followed by "area". The first value specifies the total wall area of chamber. The second value specifies the area of floor. Both values should be in terms of [cm^2]. Default values are 6.0E4 and 1.0E4 [cm^2] for *area* and *floor*, respectively.

11th array: *end of input file* (Required)

"end" -Character string "end" specifies that this is the end of the input file.

A.3. CAEROT SAMPLE INPUT FILE AND DESCRIPTION

A.3.1 Sample Input file

```
grid
5.0, 185.0, 36
0.0, 60.0,   12
0.0, 150.0, 30

group
2
5
0.1, 0.3, 0.4, 0.5, 1.0, 2.0

source
1
0.503, 1.018928, 3.518586E-6
1
60.67, 63,33, 30.67, 33.33, 41.0, 41.0
270.0, 60.0, 120.0

time
700.0

velocity
ut835.dat
vt835.dat
wt835.dat

sample
1
111.0, 112.0, 31.0, 31.2, 83.0, 83.0
16.67

bkg
0
0.02
end
```

A.3.2. Input File Description

1st array: *computational domain and grid size* (Required)

"grid" -Character string "grid" indicates that the following three sets of triplets specify the computational domain and grid size. Each triplet must be written as a separate record.

xi, xmax, nx -These values specify the domain of the x-coordinate and the number of the nodes in the x-direction. The values, *xi* and *xmax*, should be real numbers, and *nx* should be an integer value. *Xi*, and *xmax* is the starting and end point of the computational domain in the x-direction, and *nx* is the number of the nodes in the x-direction.

yi, ymax, ny -These values specify the domain of the y-coordinate and the number of the nodes in the y-direction. The values, *yi* and *ymax,* should be real numbers, and *ny* should be an integer value. *Yi*, and *ymax* is the starting and end point of the computational domain in the y-direction, and *ny* is the number of the nodes in the y-direction.

zi, zmax,nz -These values specify the domain of the z-coordinate and the number of the nodes in the z-direction. The values, *zi* and *zmax*, should be real numbers, and *nz* should be an integer value. *Zi*, and *zmax* is the starting and end point of the computational domain in the z-direction, and *nz* is the number of the nodes in the z-direction.

2nd array: *group sectionalization* (Required)

"group" -Character string "group" indicates that the following sequence of

numbers are used for group boundaries. The format is same as the one for SAEROSA.

3rd array: *source specification* (Required)

"source" -Character string "source" indicates that the following set of values are for source particle specification. The source distribution is assumed to be the log-normal distribution.

N_mode -This integer value specifies the number of mode. *N_mode* sets of values must follow. Each set must contain *mdia, tvol, stdv, srflg, vflx, ti*, and *tf* parameters.

mdia, tvol, stdv - Real triplets, which describe the median diameter (*mdia*) in [μm], the total volume of particle released (*tvol*) in [cc], and geometric standard deviation (*stdv*). The triplets must be written as a separate record.

srflg -This integer value specifies the spatial dependence of the source term. This value can only be 0, or 1. This must be written as a separate record.

srflg=0 -It implies source is spatially homogeneous. Source will be added into all the nodes in the computational domain equally.

srflg=1 -It implies source is localized. The source release domain must be specified on the next record by a sequence of six real values that corresponds to *(xmin, xmax, ymin, ymax, zmin, zmax*). Currently, only one source is supported by the code.

vflx, ti, tf -Real triplet that specifies the volume flux of the source, and the time

interval of the source. This must be followed by *srflg* as a separate record. When *vflx* is zero, it implies that the source does not carry an initial momentum. When *ti*, and *tf* are both zero, it implies the source is initially distributed into source release domain. When *ti*, and *tf* is not zero, but both are the same values, the code assumes that the entire source is released instantaneously into the source domain. Value of *vflx* should be written in terms of [cc/sec], and those of time interval should be in terms of [sec]. Note that the volume flux is not flux of source particle, but it is the volume flux of air, carrying the aerosol.

4th array: *simulation time* (Required)

"time" -Character string "time" indicates that the following value is for the simulation time.

twfin -This real value specifies the simulation time in terms of [sec].

5th array: *velocity file specification* (Required)

"velocity" -Character string "velocity" indicates that the following three character strings are name of the velocity file. The order of the velocity files must be x, y and z-components, respectively. Each velocity file name must be written as a separate record.

6th array: *particle sampling scheme* (Optional)

"sample" -Character string "sample" indicates the following sets of values specify the particle sampling location and its rate.

smpflg -This integer value specifies the sampling method. This value must be 1, or 2.

smpflg=1 -There exists a sampling or sink domain that actually removes aerosol particles from the computational domain. Then, it should be followed by two records of values. The first record specifies the sampling domain by six real values (*xmin, xmax, ymin, ymax, zmin, zmax*) in terms of [cm]. The second record specifies the sampling volume flux in terms of [cc/sec]. This value should be real and it is volume flux of air, not that of the aerosol particles.

smpflg=2 -This indicates that there are no physical removal of aerosol particles from the computational domain, but a separate output file will be created which shows the concentration of the aerosol in a domain specified in the next record as *(xmin, xmax, ymin, ymax, zmin, zmax*). This is mostly for a diagnostics purpose.

7th array: *background particle* (Optional)

"bkg" -Character string "bkg" specifies that the following values specify the presence of the background aerosol. Background particle distribution is assumed to be same distribution as the urban condition of the atmospheric aerosol in table 5.

bkgflg -This integer value specifies whether there exist background particles in the computational domain. The value can only be 0, or 1.

bkgflg=0 -There are background particles in the computational domain. A

real value must follow after bkgflg, which represents the fraction of the background particle concentration compared to the volume concentration shown in table 5.

bkgflg=1 -There is no background particles.

8th array: *solid wall specification* (Optional)

"wall" -Character string "wall" indicates that the following sets of numbers are specifications of the solid wall boundary. When the grid is specified in the first array, the code assumes that the computational domain is surrounded by solid walls. In this array, user can specify solid wall boundaries inside the computational domain to produce a complex geometry.

nw -Number of solid boundaries that the user would specify. This should be an integer value.

ii, jj, kk, mm - *Nw* sets of four integer values must be given following *nw,* as separate records. These specify the locations of solid boundaries. The values *ii, jj, kk* give the node number, and *mm* specifies the of unit normal of the surface.

mm=1 -Solid boundary is created with unit normal in -x direction.

mm=2 -Solid boundary is created with unit normal in +x direction.

mm=3 -Solid boundary is created with unit normal in -y direction.

mm=4 -Solid boundary is created with unit normal in +y direction.

mm=5 -Solid boundary is created with unit normal in -z direction.

mm=6 -Solid boundary is created with unit normal in +z direction.

9th array: *open boundary specification* (Optional)

"nowall" -Character string "nowall" indicates that the following sets of numbers specify the open boundary location.

nnw -Number of open boundaries that the user would specify. This should be an integer value.

ii, jj, kk, mm - *Nnw* sets of four integer values must be given following *nnw,* as separate records. These specify the locations of open boundaries. The values *ii, jj, kk* give the node number, and *mm* specifies the of unit normal of the surface.

mm=1 -Open boundary is created with unit normal in -x direction.

mm=2 -Open boundary is created with unit normal in +x direction.

mm=3 -Open boundary is created with unit normal in -y direction.

mm=4 -Open boundary is created with unit normal in +y direction.

mm=5 -Open boundary is created with unit normal in -z direction.

mm=6 -Open boundary is created with unit normal in +z direction.

10th array: *temperature specification* (Optional)

"temp" -Character string "temp" indicates that the following value is the temperature of air. Default value is 300 K.

temp -This real value specifies temperature of air in terms of K.

11th array: *density of particle specification* (Optional)

"dens" -Character string "dens" indicates that the following value is the density of

particles. Default value is 1.0[g/cc].

den -This real value specifies the density of aerosol particles in terms of [g/cc].

12th array: *viscosity of air specification* (Optional)

"vis" -Character string "vis" indicates that the following value is the viscosity of air. Default value is 1.83E-4 [kg/cm/s]

vis -This real value specifies the viscosity of air in terms of [kg/cm/s]

13th array: *end of input file* (Required)

"end" -Character string "end" specifies that this is the end of the input file.

VITA

HyeongKae Park graduated from Kumagaya High School, Saitama, Japan, in March 1997. He attended University of Oregon, Eugene, Oregon, from January 1998 to June 2001 to obtain bachelor of science degree in chemistry and physics. He attended Louisiana State University, Baton Rouge, Louisiana, in August 2001 to pursue his graduate degree. He is currently a master's degree candidate in the Department of Physics and Astronomy/Nuclear Science Center with Health Physics option.